JOURNAL OF GEOPHYSICAL RESEARCH, VOL. 113, E09004, doi:10.1029/2007JE003005, 2008

Click Here for Full Article

Constraints on the elastic thickness, heat flow, and melt production at early Tharsis from topography and magnetic field observations

A. M. Jellinek,[1] C. L. Johnson,[1] and G. Schubert[2]

Received 12 September 2007; revised 16 April 2008; accepted 19 June 2008; published 11 September 2008.

[1] The southern half of the Tharsis region of Mars displays enigmatic variations in the crustal magnetic field that are correlated with topography and the distribution of volcanism. Radial magnetic field anomaly values (B_r) at 400 km altitude are greater than 25 nT over areas at elevations less than about 6 km, $B_r = 0$ over areas at higher elevations where volcanism is also concentrated. Assuming that much of the uplift and magmatism of Tharsis postdates the crustal magnetic field, we hypothesize that the absence of radial field in the central part of the rise is related to enhanced heat flow from an underlying mantle plume. A parameterized mantle convection model, combined with a heat transfer requirement for crustal demagnetization and analysis of the dynamic topography provides restrictive and self-consistent constraints on the plume structure, excess temperature ΔT_{ex} and heat flux q_p as well as the average elastic thickness d_e at Tharsis at the time of uplift. These results lead, in turn, to bounds on the long-term average magma supply from the mantle. ΔT_{ex} is found to be in the range 205–240°C and upper bounds for d_e are 29–40 km, depending on the magnitude of the dynamic topography. Assuming magnetite is the dominant magnetic carrier, these results imply also that the lower 50–60% of the crustal column is raised above the Curie temperature and thermally demagnetized. The plume heat flux $q_p \approx 60$–100 mW m^2 and corresponds to melt production rate $Q \approx 0.01$–0.03 km^3 a^{-1}, comparable to minimum estimates determined from geological data for the rate of Noachian-Hesperian volcanism.

Citation: Jellinek, A. M., C. L. Johnson, and G. Schubert (2008), Constraints on the elastic thickness, heat flow, and melt production at early Tharsis from topography and magnetic field observations, *J. Geophys. Res.*, *113*, E09004, doi:10.1029/2007JE003005.

1. Introduction

[2] One of the most interesting observations of the surface of Mars is the concentration of large shield volcanoes on the Tharsis rise, where the majority of the planet's volcanism has occurred over the planet's 4.5 Ga evolution. It has been suggested on geological grounds that the rate of volcanism was particularly intense in the early part of Mars' history (i.e., the Noachian and early Hesperian epochs) but has declined significantly over time [*Greeley and Schneid*, 1991]. This picture is consistent with a significant reduction in mantle heat flow inferred from an increase in average elastic thickness through time [*Zuber et al.*, 2000; *McKenzie et al.*, 2002; *McGovern et al.*, 2002] and is expected from thermal evolution models [e.g., *Kiefer*, 2003; *O'Neill et al.*, 2007]. The thermal and volcanic history of early Tharsis bears on two issues of particular interest. First is the relationship between the rate of volcanic outgassing and the production of an atmosphere sufficiently dense and warm to permit liquid water at the surface in the Noachian [*Forget and Pierrehumbert*, 1997; *Jakosky and Phillips*, 2001; *Manning et al.*, 2006; *O'Neill et al.*, 2007]. Second is the temporal relationship between the uplift of Tharsis and a now extinct Martian dynamo, which remains a matter for debate [*Nimmo and Stevenson*, 2000; *Schubert et al.*, 2000; *Arkani-Hamed,*, 2004; *Williams and Nimmo*, 2004; *Johnson and Phillips*, 2005; *Lillis et al.*, 2008a, 2008b]. In particular, does the enhanced volcanism at Tharsis imply a magnitude of core heat loss sufficient to drive a dynamo [*Stevenson*, 2001; *Williams and Nimmo*, 2004] potentially beyond the Noachian epoch? Alternatively, might such a mantle upwelling impart a spatially localized "patch" of high heat flux on the core-mantle boundary that could act to destabilize or extinguish a preexisting dynamo (B. Sreenivasson and A. M. Jellinek, manuscript in preparation, 2008)? The mantle dynamics that might give rise to the localization and remarkable longevity of Tharsis volcanism, as well as its evolution in intensity over time, remain poorly understood. Hypothetical models in which long-lived upwellings have emerged include effects related to a possible spinel-perovskite phase change [*Harder and Christensen*, 1996] and to mantle layering [*Wenzel et al.*, 2004]. However, both pictures can imply differing heat transfer properties for mantle upwelling into the Tharsis region and neither picture is easily or uniquely reconciled with the rates of mantle melting and volcanism inferred for early Tharsis.

[1]Department of Earth and Ocean Sciences, University of British Columbia, Vancouver, British Columbia, Canada.
[2]Department of Earth and Space Sciences, University of California, Los Angeles, California, USA.

Copyright 2008 by the American Geophysical Union.
0148-0227/08/2007JE003005$09.00

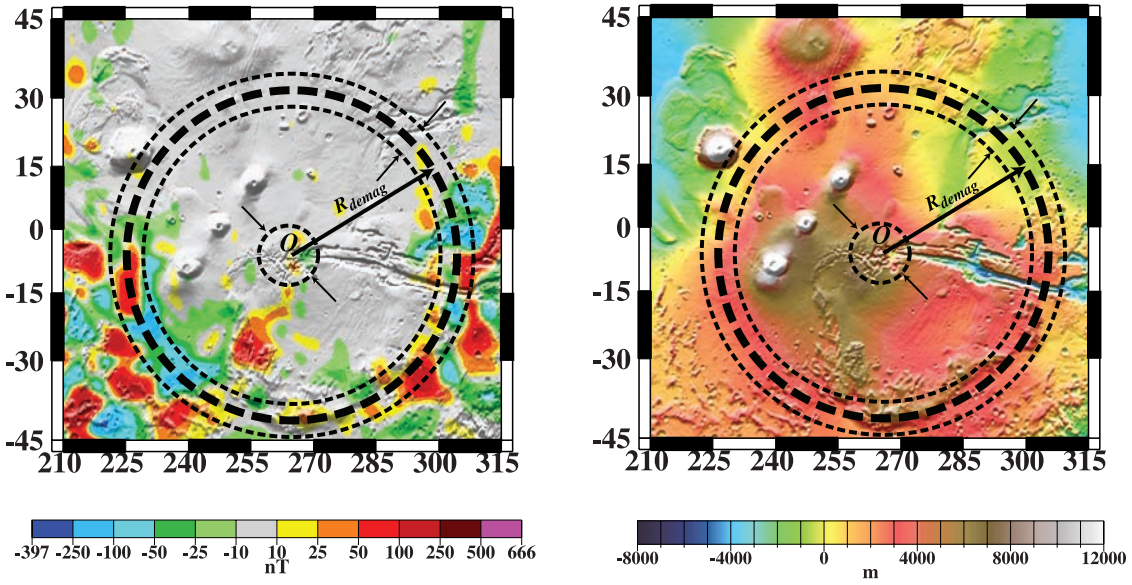

Figure 1. Maps showing (left) radial magnetic field anomalies B_r after *Langlais et al.* [2004] and (right) topography from Mars Orbiting Laser Altimetry (MOLA) data for the Tharsis region. Whereas strong magnetic fields occur below 6–7 km in the southern half of the approximately axisymmetric bulge, virtually no magnetic fields are observed at higher elevations. Thick lines indicate the radius of the demagnetized region as defined from the center of the topographic bulge *O* (small dashed circle). Thin lines indicate the uncertainties on the center of the bulge and on the radius of the demagnetized region. The absence of magnetized crust north of the dichotomy boundary is discussed in the text.

[3] A key constraint that is currently missing for thermal evolution models of early Mars, and a primary motivation of this work, is a reliable estimate of the Noachian heat flow through the Tharsis region. Figure 1 shows a provocative spatial correlation between the pattern of crustal magnetic anomalies B_r and topography at Tharsis that may provide a clue to understanding the heat flow and melt production in this region. Magnetic field anomalies at 400 km altitude over the southern half of Tharsis have magnitudes that are independent of azimuth but they are generally absent above an elevation of ~6 km. The major exception to this is the presence of anomalies at high elevations over Claritas Fossae as noted by *Johnson and Phillips* [2005]. The ratio of the radius of this annular demagnetized region r_d to the radius of Tharsis R_{th} is about 0.6–0.7. Directly above altitudes ≤6 km anomalies are large (>25 nT). On the basis of several previous studies [e.g., *Arkani-Hamed*, 2004; *Johnson and Phillips*, 2005] we hypothesize that the absence of magnetic field anomalies at satellite altitude reflects thermally demagnetized crust. We assume that prior to the emplacement of the Tharsis plume the lateral and vertical distribution, along with the type of magnetic carriers are homogeneous over the region. In other words, the absence of magnetic anomalies above central Tharsis and the presence of strong anomalies below the 6 km altitude contour are not intrinsic properties of the geology of the crust or solely a consequence of upward continuation of the surface field to spacecraft altitude. We note that no magnetic anomalies are observed over the northern half of Tharsis, an intriguing feature that we discuss below.

[4] A popular model for the origin of Tharsis is that the uplift and construction of the topographic swell as well as the associated volcanism are related to a mantle plume [*Harder and Christensen*, 1996; *Schubert et al.*, 2001; *Solomon et al.*, 2005; *Williams et al.*, 2008]. That volcanism has apparently persisted from the Noachian over much of the planet's history suggests that such a thermal upwelling must also be spatially stable over time scales larger than that for mantle convective overturn. The precise timing of this plume relative to the proposed early dynamo is unknown. If the arrival of the Tharsis plume at the base of the lithosphere postdated crustal magnetization by an internal magnetic field, as suggested by recent work [*Lillis et al.*, 2008a, 2008b], then the absence of magnetic anomalies over areas with elevations higher than 6 km supports a hypothesis that the uplift of Tharsis was associated with the thermal demagnetization of the central part of the region. As discussed by *Johnson and Phillips* [2005], it is possible that the earliest phase of Tharsis magmatism was contemporaneous with the end of a dynamo period. The important assumptions for our model are simply that Noachian-aged magnetized crust present beneath much of Tharsis was exposed to an increased heat flux due to the Tharsis plume. On the basis of the observed magnetization in the southern highlands it is likely that much of this was preexisting Noachian crust, but at least some of the sub-Tharsis crustal column could have been magnetized during the earliest stages of Tharsis magmatism.

[5] Enhanced heat transfer from such a localized upwelling would raise the level of the Curie isotherm in the lithosphere and also smooth intrinsic lateral variations in magnetic crustal structure, depending on the radial thermal structure of the plume. In general, the absence of magnetic anomalies could reflect a large reduction in the depth-integrated magnetization, unmagnetized crust, or crust that

is magnetized but over spatial scales much shorter than the altitude of the Mars Global Surveyor (MGS) satellite.

[6] Given this scenario and constraints on an appropriate Curie temperature for the crust, the presence and radius of the demagnetized region provides a way to probe the vertical temperature gradients across the underlying crust in the Noachian, as well as the plume structure and excess temperature. Our hypothesis for the thermal demagnetization of Tharsis crust contrasts with a popular class of explanations involving hydrothermal circulation near the volcanoes themselves [*Nimmo*, 2000; *Harrison and Grimm*, 2002; *Smrekar et al.*, 2004; *Ogawa and Manga*, 2007]. It should be noted that the two explanations are not mutually exclusive and that both processes may occur together in a given region. However, it is not straightforward to explain the pattern of demagnetization in Figure 1 (right) as a result of the superposition of hydrothermal effects due to volcanoes that are concentrated predominantly on the western half of Tharsis.

[7] A plume heat flux that causes the observed crustal demagnetization corresponds also to a thermal buoyancy force imparted to the base of the lithosphere. The topographic response to such an applied load is diagnostic of the flexural rigidity of that part of the lithosphere that deforms elastically on geologic time scales (i.e., the "the elastic thickness") [*Watts*, 2001]. In principle, the height of the present-day Tharsis bulge consequently enables an estimate of the elastic thickness, provided the fraction of the topography that is supported flexurally can be identified [e.g., *Zhong and Roberts*, 2003; *Roberts and Zhong*, 2004]. The current maximum height is presumably less than in the Noachian, consistent with the subsequent decline in the rate of volcanism and associated heat flow. However, this elevation does indicate a lower bound value. Here, we propose that joint consideration of plume heat flux conditions for thermal demagnetization and related flexure of the lithosphere is a powerful method for analyzing the early heat flow and elastic properties of this region in a self-consistent way. Results can, in turn, be applied further to provide additional constraints on the rate of mantle melt production and volcanism.

2. A Model

[8] Our model has three components that we apply to explain three observations, which are the occurrence and lateral scale of the demagnetized region, and the dynamic topography of the Tharsis rise at the time of uplift. We begin in section 2.1 by defining a reasonable picture of the thermophysical state of the pre-Tharsis mantle and lithosphere as well as the magnetic and elastic properties of the crust in the Tharsis region. In section 2.2, we build on this initial condition and develop a thermomechanical model for the formation, rise and spreading of a starting plume beneath the lithosphere, as well as the subsequent establishment of a single long-lived plume conduit beneath the Tharis region. We use our thermomechanical model to investigate the elevation of the Curie isotherm, as a function of radial distance from the plume center. We parameterize this effect via a depth fraction f, the ratio of the depth to the Curie isotherm after and before heating due to the plume. We investigate the thermal conditions need to achieve a specified f for a given magnetic mineralogy in sections 2.3 and 3.1, and discuss the implications for the observed magnetic anomaly signature of Tharsis in section 4.2. In section 2.3 we analyze the flexural support for the dynamic topography at Tharsis at the time of uplift to estimate an elastic thickness. The fraction of the topography that is related to the Tharsis plume is a second free parameter that must be specified to close the model. Existing thorough analyses of the present-day support for the Tharsis rise will provide a lower bound for Noachian dynamic topography. Notation and values for all parameters used are given in Table 1.

2.1. The Pre-Tharsis Mantle and Lithosphere

[9] The thermomechanical state and magnetic properties of the pre-Tharsis Martian crust and lithosphere are governed by the surface temperature, the rheology of the rocks, the Curie temperatures of the magnetic phases and the heat transfer properties of the underlying convecting mantle. Assuming that surface water was present in the Noachian, as suggested by varied geological observations [*Christensen*, 2005; *Bibring et al.*, 2006] and true polar wander calculations [*Perron et al.*, 2007], we take the surface temperature to be approximately 0°C, consistent with the climate modeling results of *Forget and Pierrehumbert* [1997]. The Noachian Martian mantle is assumed to be convecting at high Rayleigh number, $Ra = 4 \times 10^6$, in a stagnant lid regime resulting in a geothermal gradient across the lithosphere of $\sim$15 K km^{-1} [*Schubert et al.*, 2001; *Kiefer*, 2003]. Here, $Ra = \rho_m g \alpha \, (T_{cmb} - T_s) \, h_m^3 / \mu_o \kappa$ characterizes the vigor of the convection driven by core-cooling alone. Here, ρ_m and h_m are the mantle density and depth, g is the gravitational acceleration, α is the thermal expansion coefficient, and κ is the thermal diffusivity. Under these conditions the interior mantle will be thermally well mixed and characterized by an adiabatic temperature gradient of approximately 0.18 K km^{-1} [e.g., *Kiefer*, 2003]. The nonadiabatic temperature drop from the core-mantle boundary to the surface, $(T_{cmb} - T_s)$, is taken to be 1500°C and corresponds to a core-mantle boundary temperature of about 1820°C. This value is consistent with plausible conditions for an early dynamo, a prerequisite condition for a magnetic field to exist prior to the onset and establishing of the Tharsis mantle plume [*Nimmo and Stevenson*, 2000; *Williams and Nimmo*, 2004].

[10] We take the lithosphere to be viscoelastic (Figure 2a). More precisely, for the given geotherm and convective stress regime the lithosphere will deform in an effectively viscous way approximately where temperatures $T_v \geq 600$°C [*Watts*, 2001; *O'Neill et al.*, 2007] and in an effectively elastic way at colder temperatures. The thickness of lithosphere that behaves elastically on geological time scales is the elastic thickness d_e. The thickness of the lithosphere d_L in the stagnant lid regime depends on the mantle rheology and particularly on the nature and magnitude of the temperature dependence of the mantle viscosity [e.g., *Solomatov and Moresi*, 2000] for which there are few constraints. We take the ratio $d_e/d_L = 0.4$, which is similar to values inferred for the Hawaiian lithosphere [*Watts*, 2001]. The crustal magnetic field is taken to be carried predominantly by a petrologically plausible concentration (0.2–0.4 vol %) of single-domain magnetite grains [*Dunlop and Arkani-Hamed*, 2005], characterized by a Curie temperature, $T_c = 580$°C. It

Table 1. Parameters and Notation Used in Calculations[a]

Parameter	Value	Units
Radial magnetic field B_r	–	nT
Radius of Tharsis bulge R_{th}	1.5×10^6	m
Demagnetized radius r_d	$3 \times 0.9–1.2 \times 10^6$	m
Nusselt number Nu	–	–
Rayleigh number Ra	–	–
Surface temperature T_s	0	°C
Mantle temperature T_m	1500	°C
Hot thermal boundary olayer thickness δ_h	–	m
Initial radius of plume head R_o	–	m
Squeeze layer thickness δ_{sq}	–	m
Plume conduit radius r_c	–	m
Plume conduit thermal halo r_h	–	m
Radius of lithospheric footprint r_s	–	m
Fractional reduction in plume head height ε	–	–
Time scale for plume head spreading τ_{sp}	–	s
Characteristic Stokes spreading time τ_{st}	–	s
Vertical diffusion length scale during spreading z_{sp}	–	m
Elastic thickness d_e	–	m
Lithosphere thickness d_L	–	m
Isotherm for elastic thickness T_v	600	°C
Curie temperature for magnetite T_c	580	°C
Magnetized crust thickness d_m	–	m
Max. plume excess temperature ΔT_{ex}	–	°C
Radial position in plume conduit or footprint r	–	–
Background mantle viscosity μ_o	5×10^{21}	Pa s
Mantle viscosity $\mu(T)$	–	Pa s
Rheological temperature scale γ	0.023	$°C^{-1}$
Plume temperature at centerline T_p	–	°C
Plume excess temperature ΔT	–	°C
Mean plume excess temperature $\langle \Delta T \rangle$	–	$°C^{-1}$
Reference rise velocity V_o	–	m s^{-1}
Gravitational acceleration g	3.70	m s^{-2}
Thermal expansion coefficient α	3×10^{-5}	$°C^{-1}$
Mantle density ρ	3400	kg m^{-3}
Specific heat C_p	800	J kg^{-1} $°C^{-1}$
Thermal conductivity K	4	W m^{-1} $°C^{-1}$
Critical magnetic crust thickness d_{cr}	–	m
Critical thickness ratio f	–	–
Plume conduit radius r_c	–	m
Plume heat flux q_p	–	W m^{-2}
Geothermal gradient $T_g(z)$	15	K km^{-1}
Mantle depth h_m	1.76×10^6	m
Flexural rigidity D	–	N m
Dynamic topography h_t	–	m
Lithosphere-mantle density difference $\Delta \rho_m$	3	%
Elastic modulus E	$5.5 \times 10^{10} – 3 \times 10^{11}$	Pa
Poissons ratio v	0.25	–
Vertical position in melt region z	–	m
Mantle solidus temperature $T_{sol}(P)$	–	°C
Pressure P	–	GPa
Height of melting region Z_m	–	m
Volumetric melt production rate Q_m	–	km^3 a^{-1}
Mantle melt fraction Γ_m	–	–
Lithosphere melt fraction Γ_L	–	–

[a]Except where indicated in the text all parameters are taken from *Schubert et al.* [2001], *Zhong and Zuber* [2001], *Kiefer* [2003], and *O'Neill et al.* [2007].

should be noted that the effective T_c depends on the concentration and distribution of all magnetic minerals present, which remains poorly understood for Mars [e.g., *Dunlop and Arkani-Hamed*, 2005] and a matter for debate. If alternative magnetic carriers are assumed, such as pyrrhotite (T_c = 320°C), titanomagnetite (T_c = 150–300 4°C), titanohematite (T_c = 530–650°C), or hematite (T_c = 675°C), then the relationship between T_v and T_c must be adjusted accordingly. We choose magnetite as a dominant carrier because for petrologically reasonable concentrations in Martian volcanic rocks it is straightforward to explain a crustal field that is on average greater than Earth's 50 μT field. In addition, because $T_v \approx T_c$ we take the thickness of magnetized crust $d_m \approx d_e = 0.4 d_L$.

2.2. A Mantle Plume Beneath Tharsis

[11] The thermal and mechanical response of the Martian lithosphere to a mantle plume depends on the flow and heat transfer properties of the upwelling. A hot, low-viscosity mantle plume rising from an unstable thermal boundary layer at the core-mantle boundary is expected to have a large head and narrow underlying tail or conduit through which hot mantle is continuously supplied [e.g., *Jellinek and Manga*, 2004]. The evolution of plume-lithosphere thermal interactions can be generally regarded in two stages (Figure 2). Initially, an ascending spherical plume head will approach the lithosphere and spread laterally beneath an overlying "squeeze layer", becoming increasingly planar at its upper and lower surfaces over time (Figure 2b). In the reasonable limit that the lithosphere behaves as an approximately rigid boundary the diameter of the head is expected to increase at a rate approximately proportional to $\sim t^{0.26}$ (t is time), whereas the head height and squeeze layer thickness decline as $\sim t^{-0.56}$ and $\sim t^{-0.5}$ [*Griffiths and Campbell*, 1991]. This evolution in head geometry and squeeze layer thickness implies a spatially complicated and time-dependent thermal coupling to the lithosphere. If the rheology of the lithosphere is such that viscous stresses arising in response to the spreading cause concomitant erosion of the lithosphere, resulting in a topographic "footprint", the picture becomes still more complicated (Figure 2b) [e.g., *Olson et al.*, 1988; *Davies*, 1994]. The nature of the time dependence of the spreading should, however, be preserved for most geophysically plausible situations in which the effective viscosity of the lithosphere is much larger than that of the upwelling.

[12] Once the plume head spreads and thins to about 1/2 its initial radius, vertical temperature gradients become enhanced above the conduit, resulting in a transition to a thermal regime governed by the heat flux delivered over the surface area of the footprint by the quasi-steady upwelling of hot mantle in the conduit [*Jellinek and Manga*, 2002] (Figure 2c). This transition in thermal regime implies that the pattern of crustal demagnetization in Figure 1 may record effects related to the transient spreading of the initial Tharsis plume head as well as the subsequent quasi-steady flow in a long-lived plume conduit. Accordingly, we investigate each regime, in turn.

2.2.1. Transient Lithospheric Heating: Arrival and Spreading of a Tharsis Plume Head

[13] The magnetic anomaly data in Figure 1 are a time-integrated signal and provide no a priori way to distinguish

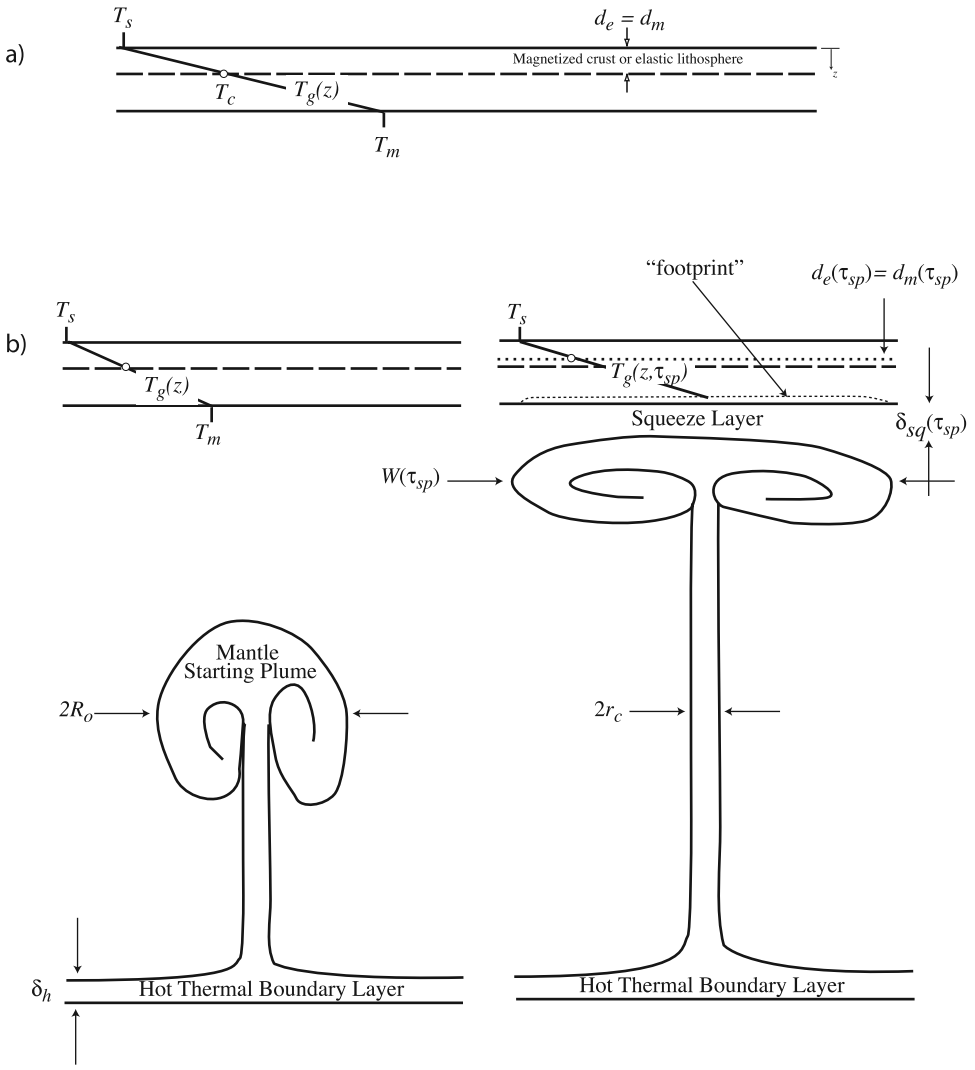

Figure 2. Definition sketches for each component of our model. (a) The initial (pre-Tharsis) thermal and magnetic state of the lithosphere. The dashed line indicates the depth of the magnetized crust, which is taken to be approximately equal to the elastic thickness. (b) The rise and time-dependent spread of a mantle starting plume beneath the Martian lithosphere. The topographic "footprint" is an expected result of thermomechanical erosion of the lithosphere on spreading of the plume head over the time to thin to about one half its initial diameter. The dotted line indicates a corresponding shallowing of the Curie isotherm in response to the transient conduction of heat from the plume head to and across the lithosphere. (c) A steady state thermal model of a Martian mantle plume conduit under steady state conditions. (d) A model for the flexural response of the lithosphere to the buoyancy force imparted by an underlying plume conduit. See text for discussion and Table 1 for notation.

effects related to the initial spreading of the plume head from the subsequent establishment of a long-lived plume conduit. However, analysis of spreading of the plume head to one half its initial thickness constrains the ultimate size of the footprint, providing a thermomechanical link to the radius of the demagnetized region. Bounds on the of crustal demagnetization that might occur during this spreading can also be estimated from the total heat transferred to, and conducted across the overlying lithosphere. The resulting increase in the average temperature $\langle T_L \rangle$ of the lithosphere implies an increase in the geothermal gradient and a corresponding shallowing of the Curie isotherm. Whether this effect can lead, in turn, to crustal demagnetization at satellite altitude is discussed in section 2.3. The magnitude of the increase in temperature depends on the heat flux from the plume head, the time scale for spreading and the evolving thermal coupling to the lithosphere during spreading. We assume that cooling of the plume head is by conduction and neglect the heat flow delivered to the lithosphere by localized intrusions of dikes and sills related to melting within the plume head and squeeze layer. However, potentially important effects related to a reduction in lateral scale length of magnetic anomalies by intrusions are discussed briefly in section 4.2.

[14] The time-dependent thermal footprint of a spreading plume head will depend on its initial size, rise velocity and

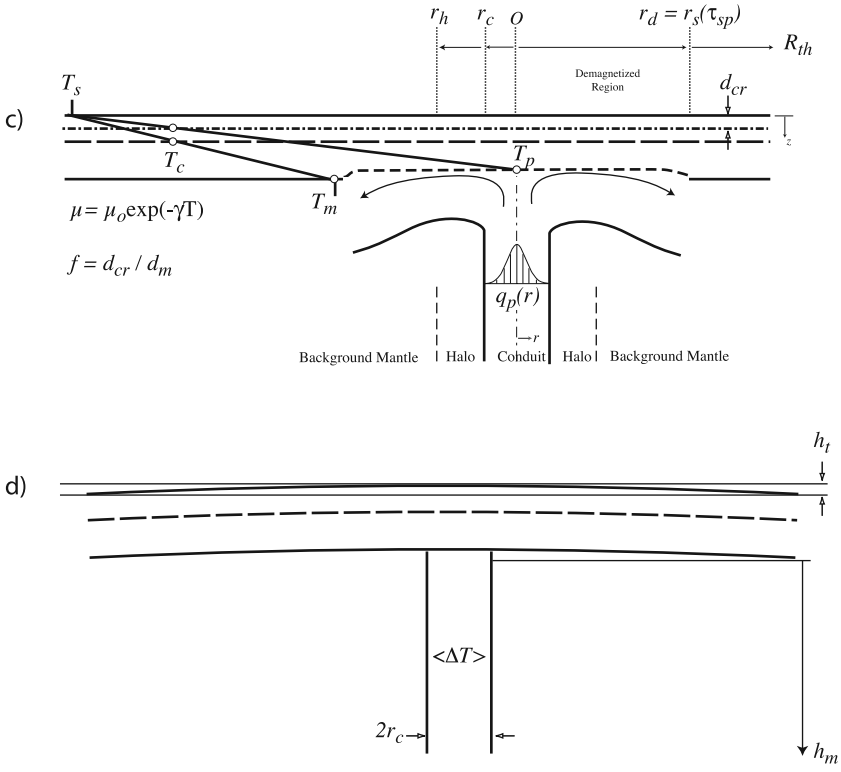

Figure 2. (continued)

spreading rate beneath the lithosphere and mantle squeeze layer (Figure 2b). The viscous response of the mantle to a rising and spreading plume is governed by the nature of the temperature dependence of the mantle viscosity. Assuming mantle deformation is in the diffusion creep limit a simplified but reasonable mantle viscosity is

$$\mu = \mu_o \exp(-\gamma \Delta T). \tag{1}$$

Here, the rheological temperature scale $\gamma^{-1} = -(d\ln\mu/dT)^{-1}$ is a constant determined from laboratory measurements on the relevant materials, ΔT is the temperature in excess of the background mantle temperature T_m and μ_o is the viscosity at the background mantle temperature (Table 1). Rock deformation experiments [*Kohlstedt et al.*, 1995] suggest that mantle viscosities will decline by $\sim$1 order of magnitude for every 100°C of plume excess temperature, implying that $\gamma \approx 0.023$°C.

[15] A mantle starting plume ascending from the core-mantle boundary is initiated where the hot conductive thermal boundary layer related to core-cooling exceeds a critical thickness

$$\delta_h = h_m / Nu, \tag{2}$$

where the Nusselt number is given by

$$Nu = 0.57(Ra/Ra_{crit})^{1/3} \tag{3}$$

and the scaling constant, modified from *Solomatov and Moresi* [2000], is broadly consistent with data from experimental studies [*Jellinek et al.*, 2003; *Gonnermann et al.*, 2004]. At middepth in the mantle, the diameter of the undeformed plume head (Figure 2b, left) $2R_o$, depends on the wavelength of the initial gravitational instability as well as inflow from below and entrainment of mantle material. On the basis of experimental measurements [*Lithgow-Bertelloni et al.*, 2001; *Jellinek et al.*, 2003]

$$R_o \approx 1.7\left(\mu_m/\mu_p\right)^{1/3}\delta_h \tag{4}$$

and the conduit radius $r_c \approx \delta_h$. Here, μ_m and μ_p are the background mantle viscosity and the plume viscosity evaluated at the maximum excess temperature ΔT_{ex}. In addition, we follow *Griffiths* [1986] and adjust this value slightly for a small additional increase in radius due to thermal effects on ascent, which is consistent in magnitude with the results of *Farnetani and Richards* [1995]. For a plume excess temperature $\Delta T_{ex} = 200$°C, comparable to that which is inferred for Hawaii, $r_c \approx \delta_h \approx 100$ km and $R_o \approx 420$ km, which is a plausible value when compared to models and inferences from hot spot swells for mantle plumes in the Earth and adjusted for the difference in mantle depth.

[16] As the plume head approaches an effectively rigid lithosphere it will flatten and spread beneath a squeeze layer that also declines in thickness over time. The time scale for the height of the plume head to decline by a fractional amount ϵ on spreading [*Griffiths and Campbell*, 1991] is

$$\tau_{sp} = (\epsilon/0.6)^{1.79}\tau_{st}, \tag{5}$$

where $\tau_{st} = (\mu_m/(\rho g \alpha \Delta T R_o))$ is the characteristic time for spreading in a Stokes flow limit. At this time the thickness of the squeeze layer

$$\delta_{sq} = 0.22 h_m \left(\tau_{sp}/\tau_{st}\right)^{-1/2} \tag{6}$$

and the lateral spread of the plume head

$$r_s = 1.3 R_o \left(\tau_{sp}/\tau_{st}\right)^{0.26}. \tag{7}$$

The vertical length scale for thermal diffusion over this time

$$z_{sp} \approx 2\left(\kappa \tau_{sp}\right)^{1/2}, \tag{8}$$

where κ is the mantle thermal diffusivity. For most conditions we analyze, $z_{sp} < \delta_{sq}$. An appropriate scale for the conductive heat flux to the lithosphere during spreading is, thus, approximately

$$q_{sp} \approx K \Delta T_{ex}/z_{sp}, \tag{9}$$

where K is the thermal conductivity, which is an upper bound because the conductive length scale is the minimum value over the evolution of the thermal regime governed by spreading. Assuming this heat flux is delivered over the full footprint of the flattened plume head over the time τ_{sp} a corresponding upper bound on the change to the mean temperature of the overlying lithosphere of thickness d_L is

$$\langle T_t \rangle = \frac{\left(q_{sp}\tau_{sp}\right)}{\rho C_p d_L} - \frac{L\Gamma_L}{C_p}. \tag{10}$$

Here, C_p and L are the specific and latent heats of lithosphere rocks. The first term on the right side is the specific heat required to raise the mean temperature of the overlying lithosphere and the second term is the consumption of latent heat related to melting a fraction of the lithosphere thickness Γ_L.

[17] The choice of appropriate values for d_L and for Γ_L requires discussion because each has a strong influence on $\langle T_t \rangle$. In the limit that the lithosphere is perfectly rigid there is no footprint and d_L is the initial value d_L°. For most plausible lithospheric rheologies and mantle viscosity models, however, some erosion is expected. *Olson et al.* [1988] find, for example, that the rise and spreading of plume heads in Earth's mantle will cause minor vertical erosion of the base of a lithosphere deforming in the diffusion creep limit (at most a few percent of the lithosphere thickness). In the Earth the extent of this erosion is expected to be enhanced in the presence of a low-viscosity asthenosphere, extending to perhaps 10–15% of the lithosphere thickness (less if the lithosphere is non-Newtonian, deforming in a dislocation limit, say). Further inspection of the *Olson et al.* [1988] results suggests that the lateral scale of the topographic footprint is set by the diameter of the plume head at $\epsilon \approx 0.5$ for most rheologically appropriate conditions, corresponding also with the transition to conduit-dominated flow discussed above. Whether Mars also has a low-viscosity zone beneath the lithosphere is unclear but cannot be discounted. In a recent analysis of the tidal dissipation within Mars from analysis of the observed secular acceleration of the nearest moon Phobos, *Bills et al.* [2005, also personal communications, 2007] require a very low average viscosity of Mars of order 10^{15} Pa s, which is at least 2 orders of magnitude less than the Earth average. They recognize that such a viscosity is unphysical for a mantle value and argue that the presence of a fluid core cannot be the full explanation. In principle these results may be explained if the tidal dissipation is concentrated within a low-viscosity layer in the upper mantle such as an asthenosphere, or in the crust. With these considerations we assume that a shallow topographic footprint is inevitable and may extend vertically over at most a few percent of the lithosphere thickness such that $d_L^\circ > d_L > 0.95 d_L^\circ$.

[18] The magnitude of lithospheric melting during spreading depends on the solidus temperature of the lithosphere and crust, which are not constrained. Consequently, it is unclear how to include even gross effects of melting in this calculation. An upper bound on the effect of transient heat transfer from a plume head on the mean temperature of the lithosphere can, however, be estimated without including melting. Assuming a 100 km thick lithosphere and ΔT_{ex} = 200°C, say, an extent of flattening ϵ = 0.5 corresponds to a time $\tau_{sp} \approx 2.7$ Ma resulting in a ≈10°C rise in the mean lithosphere temperature and a <2% increase in the geothermal gradient (Figure 3). Assuming magnetite is the magnetic carrier, such an increase corresponds only to a ~0.4 km shallowing of the Curie isotherm from an initial value of 38.6 km.

[19] In summary, for most reasonable plume excess temperatures the contribution of heat transfer from the plume head over the time τ_{sp} to the thermal structure of the lithosphere will be small in comparison to the much longer term influence of hot mantle upwelling in the plume conduit. Indeed we can generally neglect the effect of this transient phase on the magnetic crust thickness with little change to our analysis. A key mechanical consequence of the spreading of the plume head, however, is to establish the footprint, which ultimately sets the lateral length scale for the thermal coupling of the lithosphere to the plume conduit. We argue next that such a geometric constraint on the spreading of upwelling mantle at the base of the lithosphere governs the diameter of the demagnetized region identified in Figure 1.

2.2.2. Steady State Heat Transfer Through a Long-Lived Plume Conduit

[20] In a conduit-dominated thermal regime a quasi-steady upwelling of hot mantle material impinges the lithosphere and spreads laterally as a gravity current driven by a fixed buoyancy flux from the plume conduit. As discussed above, laboratory experiments and numerical simulations suggest that this lateral flow will be confined within the topographic footprint of the initial spreading plume head at the lithosphere base [*Olson et al.*, 1988] (Figure 2c). Consequently, provided the time scale for lateral flow across the footprint is much shorter than the time scale for thermal diffusion across the lithosphere the surface area over which the plume heat flux is delivered will scale as $r_s(\tau_p^\epsilon = 0.5)$ and, thus, set the radius of the demagnetized region r_d. This link between the pattern of crustal demagnetization observed at spacecraft altitude and the structure of the plume head will provide a restrictive

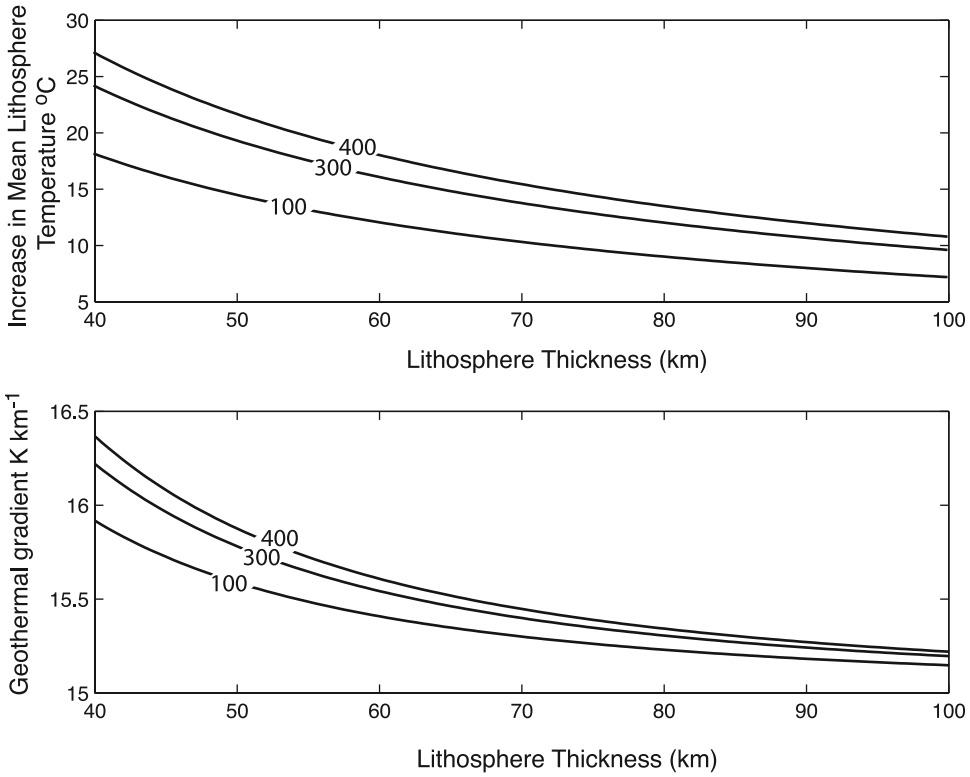

Figure 3. Plots showing (top) the increase in the mean temperature and (bottom) geothermal gradient in the lithosphere as a function of initial plume excess temperature. Calculations assume thermal conduction to the lithosphere over the time for a plume head to spread to one half its initial height (see text for discussion).

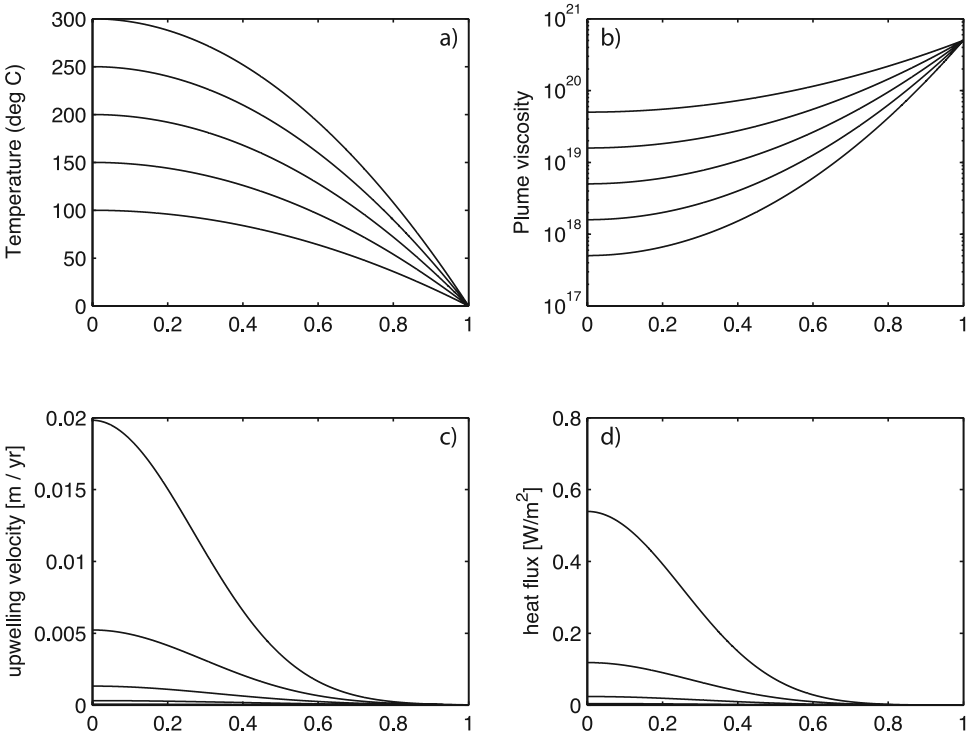

Figure 4. Plots indicating the (a) temperature, (b) viscosity, (c) upwelling velocity, and (d) heat flux as a function of radial position in the active part of the model plume conduit.

constraint on the plume excess temperature in addition to that which is found from a joint consideration of crustal thermal demagnetization and flexural support of topography.

[21] To model the steady state structure and heat transfer properties of the flow in the tail of the plume, we follow *Loper and Stacey* [1983] and *Olson et al.* [1993]. We take the Tharsis mantle plume to be an axisymmetric upwelling from the core-mantle boundary characterized by a maximum plume excess temperature ΔT_{ex} evaluated at the center of the structure ($r = 0$), and a Gaussian temperature variation (Figure 4a). As a result of the strong temperature dependence of the mantle viscosity (equation (1)) flow will be concentrated in the central 10–20% of the upwelling, forming a low-viscosity conduit of radius r_c [*Loper and Stacey*, 1983] (Figure 4b) surrounded by a diffusive thermal halo that is ~2–3 times larger [*Olson et al.*, 1993; *Kerr and Mriaux*, 2004]. The vertical heat flux related to the halo is, by definition, much smaller than that due to flow in the conduit and so it is neglected. For an established plume conduit the radius is expected to scale as $r_c \sim \delta_h$ and the flow is analogous to Poiseuille flow in a cylindrical pipe characterized by a radial temperature variations in excess of the background mantle of the form $\Delta T_{ex}(1-r^2)$ [*Olson et al.*, 1993], where r is normalized such that it is 0 at the center of the conduit and 1 at r_c. Corresponding radial velocity and plume heat flux variations in this region of the upwelling are governed by the magnitude of the radial viscosity variations and are (Figures 4c and 4d)

$$V(r) = V_o \exp(\gamma \Delta T(r)) \tag{11}$$

and

$$q_p(r) = V(r)\Delta T(r)\rho C_p, \tag{12}$$

respectively. Here, the reference upwelling velocity in the cylindrical conduit is $V_o = \rho g \alpha \Delta T_{ex} r_c^2 / 4\mu_o$ and ρ and C_p are the mantle density and specific heat.

[22] When flow from this conduit impinges and spreads along the base of the lithosphere the fastest spreading, lowest viscosity and hottest material at the center of the upwelling will be concentrated at the upper boundary of the footprint as a lubricating layer. With this resulting approximately free-slip mechanical boundary condition imposed, plume material spreads radially away from the center of the conduit over the length scale r_s, cooling progressively and resulting in a laterally varying vertical heat flux at the top of the footprint of the form [*Jellinek et al.*, 2003] (Figure 2c)

$$q_f(r) = q_p^{r=0}\left[1 - r^{1/2}\right], \tag{13}$$

where r is normalized to be 0 at the center of the conduit and 1 at r_s.

2.3. Heat Transfer and Crustal Demagnetization

[23] The plume heat flux and associated magmatism can lead to partial or complete thermal demagnetization. Elevation of the lithospheric thermal gradient may result in temperatures over part, or all, of the depth extent of the magnetized layer being raised above the Curie temperature. In the simplest case, assuming a single lateral scale length of magnetization that is larger than the spacecraft altitude and is unchanged due to the long wavelength thermal signature of the plume, the resulting magnetic field over the crust will be reduced in magnitude proportional to the fractional thickness of the magnetized layer that becomes demagnetized. The spectrum of scale lengths of magnetization is of course complex including contrasts at spatial scale lengths close to, or less than, the spacecraft altitude. Elevation of the thermal gradient in such a more complex source layer, along with reductions in scale length of the magnetization due to intrusions will further reduce the observed magnetic anomalies, possibly to below the detection threshold, even without complete demagnetization of the crust.

[24] Because quantitative assessment of changes in scale length of magnetization require a priori knowledge of the magnetization spectrum of the preexisting crust and knowledge of the distribution of intrusions relative to that layer, we model only the long-wavelength thermal effect of the plume. At steady state, lateral flow within the footprint will impart a heat flux that varies slowly over the radius r_s, and this imparts lateral temperature variations over spatial scales comparable to r_s, rather than, say, the conduit diameter $2r_c$. On the basis of the data in Figure 1a, the appropriate scale length for r_s is $O(10^3)$ km, which is significantly larger than the altitude of the MGS magnetic observations. We analyze thermal demagnetization as a result of increasing the geothermal gradient above the footprint, which will reduce the depth-integrated crustal magnetization (Figure 2c). In section 4.2 we discuss briefly effects related to reductions in the lateral scale length of magnetic anomalies that might occur as a result of magmatic intrusions.

[25] At steady state the plume heat flux $q_p(r)$ corresponds to approximately linear temperature gradients in the overlying lithosphere that are steeper than the initial geotherm $T_g(z)$ and given by (Figure 2)

$$T(r,z) = q_p(r)z/K + T_g(z), \tag{14}$$

and $T_s = 0$ at $z = 0$. Where the temperature along this profile exceeds the Curie temperature T_c, the crust will become demagnetized. For magnetite the initial depth of the magnetized layer $d_m \approx d_e$, so we can also write $d_m = 0.4\, d_L$. We define d_{cr} as the depth at which T is equal to T_c due to the elevated geotherm, and introduce f as the ratio d_{cr}/d_m. f is essentially a measure of the vertical extent of possible crustal demagnetization, with a decreasing f corresponding to a greater vertical extent of demagnetization.

[26] Taking $T_g(d_{cr}) \leq T_c$, we rearrange equation (14) to identify a critical plume heat flux condition that results in a given f at the edge of the footprint r_d, where $r_d \approx r_s$:

$$q_f^{(r \leq r_d)}(r) \frac{K}{f d_m}\left[T_c - T_g(d_{cr})\right]. \tag{15}$$

[27] Examination of equations (12)–(15) shows that for a specified mantle plume model (compare section 2.3) and T_c we can vary d_m for given ΔT_{ex} to map $\Delta T_{ex} - d_m$ regimes that result in a specified f at $r \leq r_d$. For a given Curie temperature a greater vertical extent of demagnetization (decreased f) can be achieved either by increasing the plume

heat flux or decreasing the initial background geotherm (equivalent to increasing d_m).

2.4. Lithospheric Flexure and the Tharsis Rise

[28] Because the plume conduit has a radius that is small in comparison to the depth of the mantle we can neglect membrane stresses related to Mars' lithospheric shell and treat the problem approximately in a cartesian geometry [*Turcotte et al.*, 1981]. In this regime, the topographic amplitude response of the elastic lithosphere to upwelling flow concentrated within the narrow low-viscosity part of the Tharsis plume conduit is given by [*Watts*, 2001]

$$h_t = h_m \alpha \langle \Delta T \rangle \left(\frac{1}{1 + 16 D \pi^4 / (\lambda^4 \Delta \rho_m g)} \right), \qquad (16)$$

where

$$D = \left(E d_e^3 \right) / \left(12 \left(1 - \nu^2 \right) \right) \qquad (17)$$

is the flexural rigidity and $\lambda = 4\ r_c$ is the appropriate full sinusoidal wavelength of the plate forcing for this scenario. Here E is the elastic modulus, ν is Poisson's ratio, h_t is the maximum topography supported by flexural stresses (i.e., "the dynamic topography") and $\langle \Delta T \rangle$ is the radially averaged excess temperature in the conduit. Thus, a constraint on h_t implies an elastic thickness d_e. It should be noted that in this development we ignore an additional restoring force related to the stabilizing density difference at the core-mantle boundary [*Richards and Hager*, 1984], the nature of which is unclear. We also ignore the minor contribution of membrane stresses to the dynamic support of Tharsis, consistent with results of the scaling analysis of *Turcotte et al.* [1981]. The main consequences of neglecting these effects is that the elastic thickness determined with equations (16) and (17) will be an upper bound.

[29] An observational constraint on h_t is difficult to obtain. MOLA topography provides direct information about the present maximum height of the Tharsis bulge, most of which is probably related to constructional volcanism [e.g., *Williams et al.*, 2008]. Careful modeling studies of the long-wavelength topography and geoid anomalies at Tharsis [*Zhong and Roberts*, 2003; *Roberts and Zhong*, 2004] restrict the fraction of this topography due to dynamic mantle support to be less than about 25% of the maximum value or $h_t = 1.5$–2 km, which is comparable to that which is typically inferred for Hawaii. The decline in eruption rate, and by inference heat flow, at Tharsis since the Noachian, combined with the secular cooling of the planet as a whole, suggest that both the maximum height of Tharsis and the magnitude of dynamic topography may have been significantly greater in the Noachian. Accordingly, below we examine cases for 25–50% dynamic support.

[30] Whether the uncertainty in an appropriate value for h_t influences d_e in a significant way compared to other parameters is an important issue. Examination of equation (16) in the limit $(16 D \pi^4 / (\lambda^4 \Delta \rho\ g) \gg 1)$ (i.e., the topography is not compensated) indicates

$$d_e \propto \left(r_c^4 \Delta T_{ex} / E h_t \right)^{1/3}. \qquad (18)$$

Thus, the most important parameter is r_c and factors of <1–2 change in h_t or ΔT_{ex} will cause tens of percent variations in d_e. We note that the variation in E applied in the literature has a considerably larger influence. Although typically taken to be 1×10^{11} Pa [e.g., *Comer et al.*, 1985; *Phillips et al.*, 2001; *McGovern et al.*, 2002], published values vary between 5–6×10^{10} Pa [e.g., *Heller and Janle*, 2000; *Schultz et al.*, 2004] and 1.4–3×10^{11} Pa [*Zhong and Roberts*, 2003; R.J. Phillips, personal communications, 2004], implying as much as a factor of ~2 uncertainty in estimates of d_e. Here we adopt the conventional value $E = 1 \times 10^{11}$ Pa.

[31] Noting that $r_c \approx \delta_h$ and that $r_d \approx r_s$ it is instructive to explore the sensitivity of d_e to our background mantle convection model and its link to surface observations of crustal demagnetization. Making the appropriate substitutions we find that

$$de \propto \left(\delta_h^4 \Delta T_{ex} / E h_t \right)^{1/3} \propto \left(r_d^4 \left(\mu_m / \mu_p \right)^{-4/3} \Delta T_{ex} / E h_t \right)^{1/3}. \qquad (19)$$

From equations (2) and (3), $\delta_h \sim Ra^{-1/3}$, and thus the second expression shows that d_e is influenced by the mantle Ra, albeit weakly. Through the third expression, d_e can be constrained by our observation of r_d provided that h_t is constrained and ΔT_{ex} and the magnitude of the temperature dependence of the viscosity are specified (compare equation (1)).

2.5. Plume Heat Flux and Mantle Melting

[32] Together with an estimate of the mantle solidus $T_{sol}(z)$, constraints on the average heat transfer properties of the Tharsis plume (compare sections 2.2–2.4) imply an average melt production rate in the sublithospheric plume conduit. At each vertical position in the plume conduit z, where the radially averaged temperature $\bar{T}(z)$ is greater than the solidus temperature T_{sol}, the temperature difference available to drive melting is $\Delta T_m(z) = (\bar{T}(z) - T_{sol})$. This temperature difference implies, in turn, a melt fraction $\phi(z) = C_p\ \Delta T_m(z)/L$ and a volumetric melt production rate $\Gamma(z) = \phi \bar{V}(z)\ A(z)$. Here, C_p and L are the specific and latent heats, $\bar{V}(z)$ is the radially averaged upwelling velocity, and $A(z)$ is the cross-sectional area of the plume conduit. The vertically averaged melt production rate is then

$$Q_m = \frac{1}{Z_m} \int \Gamma(z) dz, \qquad (20)$$

where Z_m extends from the depth at which $\bar{T} < T_{sol}$ to the base of the lithosphere d_L. With an additional parameterization of the fraction of melt that is erupted at the surface (i.e., an "eruption efficiency") Q_m also implies, in principle, an eruption rate [*Kiefer*, 2003; *O'Neill et al.*, 2007]. However, such a consideration is not straightforward. The initial melt may have to undergo crystal fractionation in order to become buoyant and this melt must also rise through the crust to erupt at the surface without freezing. On the basis of numerous studies of volcanism on Earth a plausible range in the ratio of intrusive/extrusive magmatism is 5–10:1 [e.g., *Crisp*, 1984].

[33] The rate of melt production is controlled by the rate of upwelling, which is particularly sensitive to the chosen mantle viscosity model, and on the solidus temperature, which is governed by the choice of bulk composition. The choice of mantle viscosity is based on studies of the Earth, and discussed above. The main uncertainties for the pre-Tharsis Martian mantle solidus are the water content and extent of the "depletion" of components extracted from the mantle to make the crust. To the extent that they are indicative of the bulk composition of early Mars the shergottite composition of Martian meteorites with possible crystallization ages ~4 Ga [*Bouvier et al.*, 2005] precludes a significant concentration of water in the melting region [e.g., *Wanke and Dreibus*, 1994]. Assuming a dry mantle, the combined experimental results of *Bertka and Holloway* [2004] and *Agee and Draper* [2004] constrain a solidus for an undepleted Martian mantle composition over a pressure range of 0–9 GPa [*Kiefer*, 2003; *O'Neill et al.*, 2007]. In contrast, in a study of the olivine Yamato 980459 meteorite, *Musselwhite et al.* [2006] establish a solidus for a depleted mantle composition. Whereas both solidii have similar slopes, the solidus temperatures at 0 GPa for the undepleted and depleted cases are $T^u_{sol}(0)$ = 1100°C and $T^d_{sol}(0)$ = 1440°C, respectively. Consistent with the findings of *O'Neill et al.* [2007] our calculations indicate that for most plausible thermal conditions these undepleted and depleted mantle solidii give unrealistically high and low rates and extents of melting, respectively. It is also not clear that the *Musselwhite et al.* [2006] solidus can be reconciled with active volcanism at Tharsis or Elysium inferred to have occurred over the last 1 Ga [*Kiefer*, 2003; *O'Neill et al.*, 2007], which suggests that this particular composition is not indicative of the bulk composition of the planet. An appropriate solidus is likely to fall between these depleted and undepleted end-member cases. Assuming that the slopes of intermediate solidii will differ only in their temperatures at 0 GPa we follow *O'Neill et al.* [2007] and take the solidus temperature $T_{sol}(P) = T^u_{sol}(P) + 200$, where P is pressure in GPa and $T^u_{sol}(P)$ is from the combined data of *Bertka and Holloway* [2004] and *Agee and Draper* [2004]. Melting rates will be enhanced in the presence of water, a small fraction of which is permitted by the shergottite composition of Martian meteorites. Our calculated melting rates based on dry compositions are, thus, plausible lower bounds. However, although plausible it is important to make clear that at present there are no unequivocal constraints on either the Martian mantle solidus or the mantle viscosity. Thus, the results of our calculations must be interpreted with caution.

3. Results

3.1. A Unique Solution for ΔT_{ex}, d_e, and r_d

[34] In Figure 5 (top) we plot elastic thickness against plume excess temperature for a range of f–h_t conditions. Also shown is the initial elastic thickness of 40 km expected from the geothermal gradient. The heavy dots are elastic thicknesses determined from solutions to equations (16) and (17) for various extents of flexural support for the Tharsis bulge. Diamonds indicate the elastic thickness (assuming $d_m = d_e$) that result in thermal demagnetization for depths greater than $d_{cr} = f\, d_m$, for a specified plume excess temperature. Where the solutions for the flexure and demagnetization calculations intersect we obtain a unique solution for both the plume excess temperature and the elastic thickness. Thus, a constraint on d_e implies a value for ΔT_{ex} or vice versa. For example, a plume excess temperature ΔT_{ex} = 200°C is consistent with an elastic thickness $d_e \approx 28$ km for 50% flexural support and implies that $f = 0.5$. If the dynamic support is reduced to 37.5% and 25%, then d_e = 33 and 38 km, respectively. Alternatively, a specific value for d_e constrains the permitted values for ΔT_{ex}, and the resulting dynamic topography and vertical extent of demagnetization. For example, a d_e of 34 km implies ΔT_{ex} = 223°C for f = 0.4 and 37.5% dynamic support. For the same d_e, lower (higher) plume excess temperatures result in less (more) dynamic support, and a lesser (greater) vertical extent of demagnetization. As a final example, if one requires that at least the lower 50% of the crustal column is raised above the Curie temperature (i.e., $f = 0.5$), for a given plume excess temperature of, say, 170°C, then $d_e \geq 29$ km and the dynamic support must be ≤37.5%.

[35] Figure 5 (bottom) shows the predicted crustal demagnetization radius r_d as a function of ΔT_{ex}, assuming as before that this length scale is set by the plume head radius r_s where the extent of spreading $\epsilon = 0.5$. The heavy dots indicate the spatial extent of the absence of magnetic anomalies observed in Figure 1 (left). Comparison of Figures 5 (top) and 5 (bottom) shows that ΔT_{ex} = 205–240°C is consistent with the topographic and magnetic observations derived from Figure 1.

3.2. Tharsis Heat Flow and Melt Production

[36] A plume excess temperature estimated from Figure 5 corresponds to an average plume heat flux and mantle melt production rate as well as extent of mantle melting shown in Figure 6. For the preferred range in excess temperature indicated $\bar{q}_p \approx 60$–100 mW m^{-2}, the melt fraction $\Gamma \approx$ 23.5–25.4% and the long-term average magma supply $\bar{Q} \approx$ 0.01–0.03 km^3 a^{-1}. This result is discussed in greater detail in section 4.1.

4. Discussion

4.1. Plume Excess Temperature, Elastic Thickness, Heat Flux, and the Magma Supply at Early Tharsis

[37] For ΔT_{ex} = 205°C, dynamic support of 50% to 25% requires elastic thicknesses of about 29 to 38 km, depending on f (Figure 7). For ΔT_{ex} = 240°C, permissible d_e values are in the range of about 31 to 40 km, also depending on f and being bounded at the high end by the pre-Tharsis value. For reasons related to the parameterization of the buoyancy force driving the elastic deformation and our neglect of the minor contribution of membrane stresses (see section 2.4) these d_e estimates are probably upper bounds. Nevertheless, these values are around one third to one half that which is inferred currently at Tharsis on the basis of local studies [*Arkani-Hamed*, 2000; *McKenzie et al.*, 2002; *McGovern et al.*, 2002] and substantially smaller than that which is estimated from the joint inversion of long-wavelength topography and geoid anomalies [*Zhong and Roberts*, 2003]. Our estimates are comparable to those inferred from local studies for Noachian regions in the southern hemisphere [*McKenzie et al.*, 2002; *McGovern et al.*, 2002], but

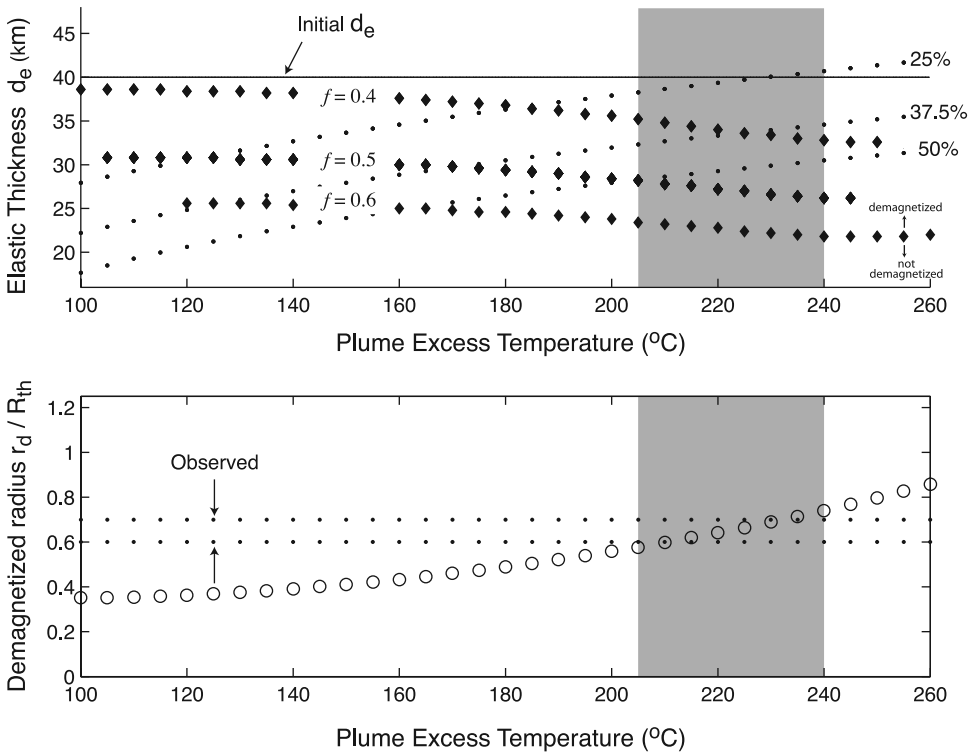

Figure 5. (top) The predicted elastic thickness d_e as a function of maximum plume excess temperature ΔT_{ex} for a range of $f - h_t$ conditions, assuming that $d_m = d_e = 0.4d_L$. Dots indicate elastic thicknesses determined from considerations of the flexural response of the lithosphere to an underlying mantle plume conduit. Solid diamonds indicate the minimum value for d_e at which the crust will appear demagnetized to an orbiting MGS satellite. (bottom) The normalized radius of the demagnetized region as a function of plume excess temperature. Open circles are values predicted on the basis of the analysis of the spreading of a mantle starting plume head beneath a rigid lithosphere in section 2.2.1. Dots are observations determined from Figure 1. The region shaded in grey indicates the range in excess temperatures for which the expected demagnetized radius is consistent with observations. See text for discussion.

smaller than the globally averaged value of $d_e > 50$ km determined for the Noachian from considerations of the rotational figure of the planet [*Daradich et al.*, 2008]. Assuming the magnetic crustal thickness is similar, our range for d_e is smaller than the 40–50 km magnetic crustal thickness inferred on the basis of rock magnetism and thermal modeling considerations [*Dunlop and Arkani-Hamed*, 2005], but is comparable with an approximately 35 km thickness determined from studies of an observed reduction in total magnetic field with crater size in impact basins greater than 500 km in diameter [*Nimmo and Gilmore*, 2001].

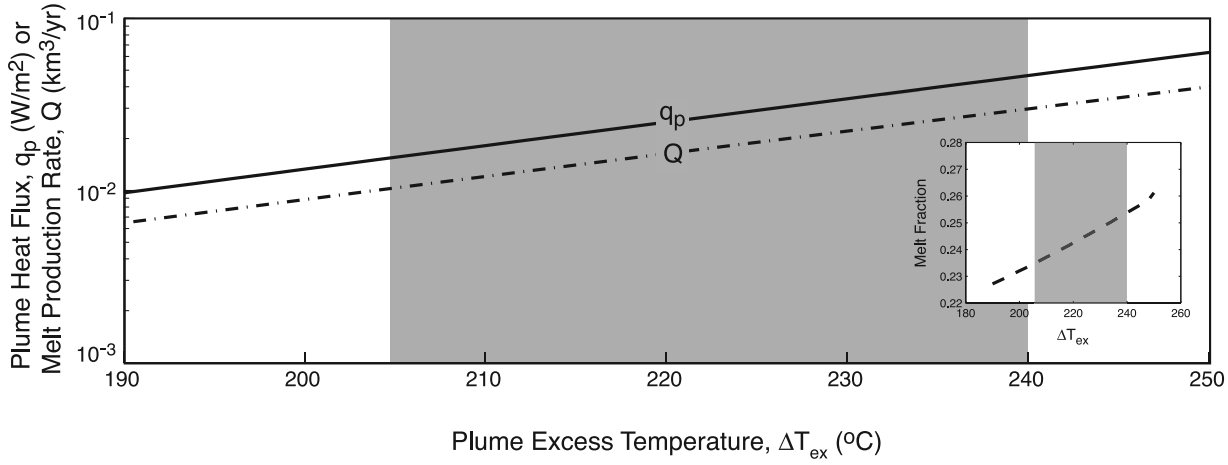

Figure 6. Plot showing the plume heat flux q (solid line), melt production rate Q (dash-dotted line), and mantle melt fraction (inset) as a function of maximum plume excess temperature ΔT_{max}.

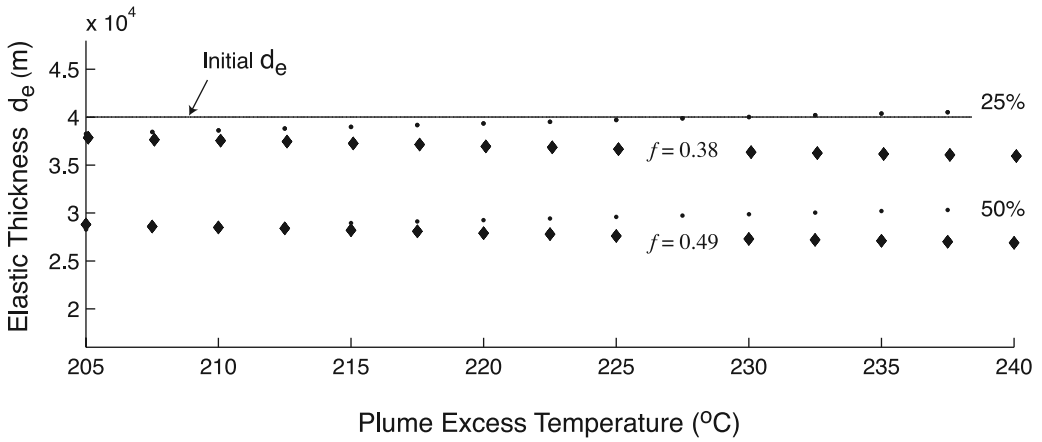

Figure 7. Plot showing the expected elastic thicknesses over a range of $f - h_t$ conditions for $205 \leq \Delta T_{ex} \leq 240$°C, the preferred excess temperatures identified in Figure 5 (bottom). Dots indicate elastic thicknesses determined from considerations of the flexural response of the lithosphere to an underlying mantle plume conduit. Solid diamonds indicate the minimum value for d_e at which the crust will appear demagnetized to an orbiting MGS satellite.

[38] From Figure 6, the corresponding long-term average magma supply $\bar{Q} = 0.01-0.03$ km^3 a^{-1} and is $\sim$1 order of magnitude greater than that inferred on geological grounds [*Tanaka et al.*, 1992; *Hartmann and Neukum*, 2001] and from models [*Kiefer*, 2003] for recent Mars volcanism. This lower bound value is also plausibly 1 order of magnitude smaller than crude estimates inferred from the total measured volume of post-Noachian volcanism but depends on the eruption efficiency applied [*Greeley and Schneid*, 1991; *O'Neill et al.*, 2007]. These melt production rates are also $\sim$1 order of magnitude less than that inferred for the Hawaiian plume [*Jellinek and DePaolo*, 2003; D.J. DePaolo, personal communications, 2007]. The average plume heat flux $\bar{q}_p = 60-100$ mW m^{-2} is similar to Noachian core heat fluxes found in thermal evolution calculations [*Hauck and Phillips*, 2002; *Williams and Nimmo*, 2004; *O'Neill et al.*, 2007]. It is also comparable to surface heat fluxes inferred from analyses of the gravity/topography admittance at Noachian regions such as the south pole [*McKenzie et al.*, 2002], Noachis Terra and NE Terra Cimmeria [*McGovern et al.*, 2002].

4.2. Crustal Demagnetization by the Tharsis Plume and Magmatic Intrusions

[39] Two end-member hypotheses can account for the spatial extent of the crustal magnetic anomalies over the Tharsis region. In the first, the absence of magnetic anomalies reflects complete demagnetization of the source layer by the thermal effect of the Tharsis plume over the region, radius r_d. In this scenario, the magnetized source region must be concentrated in the lower crust, at depths where the temperature is raised above the Curie temperature. Our estimated range for $\Delta T_{ex} - d_e$ conditions implies that $0.38 \leq f \leq 0.49$ (Figure 7). For our case of a dominantly magnetite carrier, this implies that at least the lower 50–60% of the crustal column is raised above the Curie temperature and thermally demagnetized.

[40] In a second end-member, hypothesis, crustal magnetization is concentrated in the upper crust, and is unaffected by the long-wavelength thermal expression of the plume. The absence of magnetic anomalies at spacecraft altitudes must then be due to reduction in scale length of magnetization contrasts over the Tharsis region due to the injection of dikes and sills and/or due to hydrothermal processes. The spatial distribution of dikes and sills must be related to the geometry of the melting region, which will be $\sim r_s$ in extent during the transient spreading phase of the evolution of the plume and $\sim r_c$ during the subsequent steady state conduit phase.

[41] The two mechanisms (reduction in scale length by intrusions and reduction in depth-integrated magnetization) are clearly not inconsistent with one another. However, to explain the shape and extent of the demagnetized region in Figure 1 requires intrusions emplaced during the $\sim$2–3 Ma transient phase to be distributed broadly. A zeroth-order constraint that is not known is the total volume of magma that would be required for this mechanism to work and, in particular, whether such a volume of magma is consistent with the range in plume excess temperatures we obtain from Figure 5 (bottom). A natural analog for this magmatic model on Earth is the origin of flood basalts or the mantle melting event that gave rise to, say, the Mackenzie dike swarm of western Canada. However, models addressing the melt production demanded to explain these observations with excess temperatures appropriate for Hawaii, (which are 200–300°C, comparable to what we infer for Tharsis), require specific bulk compositions to lower the mantle solidus (i.e., an eclogite component) that are peculiar to the Earth [*Cordery et al.*, 1997]. Our understanding of the Martian mantle solidus is at best incomplete, although it may be parameterized in an ad hoc way (compare section 2.5). The distribution and extent of melting in a Martian mantle plume head and the crust-mantle dynamics that govern the locations of magmatism (and thus the ultimate scale length of magnetic anomalies) are also difficult to parameterize in a meaningful way and must be modelled. This is a particularly interesting direction for future work.

4.3. Absence of Magnetic Anomalies in the Northern Hemisphere: A Constraint for *f*?

[42] The demagnetization part of the model is sensitive to the value of f applied, for which there are no direct

constraints. One indirect control on f is that temperatures within the basal part of the lithosphere will intersect the solidus for values of f much smaller than 0.4, leading to volcanism that would be presumably distributed over the southern hemisphere, which is not observed. In contrast, if f approaches unity then $d_e \approx d_m$, and the crust will become demagnetized for plume excess temperatures much smaller than are permitted by Figure 3b. Moreover, $\Delta T_{ex} < 100^{\circ}$C are insufficient to explain the rate of Noachian-Hesperian volcanism as well as maintain the Tharsis plume conduit against the action of unsteady mantle convective motions. One observation that may provide an additional clue for this parameter is the absence of magnetic anomalies on the northern half of Tharsis, as well as on the northern hemisphere in general. In a recent analysis of MOLA topography and gravity *Neumann et al.* [2004] find that the Martian crust thickness north and south of the sharp topographic dichotomy is largely bimodal, with the average southern hemisphere crust ($\sim$58 km) being about twice the average thickness of the northern hemisphere crust ($\sim$32 km). The Tharsis bulge overprints the dichotomy (Figure 1), which suggests that the emplacement of the Tharsis plume followed the formation of the dichotomy itself. Assuming that the mantle and atmosphere are thermally well stirred and at constant temperature, that the lithosphere thickness is proportional to the crust thickness, and that the crust is compositionally uniform, then the thermal gradient across the northern hemisphere lithosphere was possibly about twice as steep as that in the southern hemisphere lithosphere in the Noachian. This scenario implies that the Curie isotherm in the northern hemisphere lithosphere was about half as deep as it was in the southern hemisphere. Consequently, assuming similar radial temperature variations as in the southern part and all else being equal over the Tharsis bulge, a reasonable hypothesis for the absence of magnetic anomalies on the northern half of the region is that this reduction in magnetic crust thickness corresponds to a depth-integrated magnetization that is insufficiently large to be measured by the MGS satellite (or absent entirely). If correct, such a hypothesis suggests that $f \approx 0.5$, leading to a preferred model of $205 \leq \Delta T_{ex} \leq 240^{\circ}$C and $29 \leq d_e \leq 40$ km, depending on the extent of dynamic support (Figure 7).

5. Concluding Remarks and Future Study

[43] Assuming that the initial uplift of Tharsis postdates the crustal magnetic field we have investigated a hypothesis that the absence of radial magnetic field anomalies in the central part of the rise is related to enhanced heat flow from an underlying mantle plume. The main aim of this paper is to show how a joint consideration of the presence and spatial distribution of radial magnetic field anomalies and the dynamic topography of the Tharsis region might be used with a parameterized mantle convection model to constrain the excess temperature of an underlying mantle plume and the elastic lithosphere thickness in the Noachian epoch. Together with additional models for the composition and thermomechanical state of the mantle such constraints also give estimates of the heat transfer properties of, and melt production within, the plume. Depending on the efficiency by which melt is removed from the mantle to feed eruptions at the surface, which is not well understood but easily parameterized [e.g., *Kiefer*, 2003], this last constraint can, in turn, be compared with eruption rates inferred on geologic grounds [*Greeley and Schneid*, 1991]. Our estimates for the elastic thickness and plume excess temperature depend on the mantle convection model for early Mars, the magnitude of flexural support for the Tharsis bulge and the value for f, the critical fraction of the initially magnetized crust that must be raised above the Curie temperature such that the depth-integrated magnetization is insufficiently large to be measured by the MGS satellite. It is apparent that improved constraints on the nature of the Noachian mantle and lithosphere as well as better petrologic controls on the magnetic carriers and their vertical distribution in the Martian crust would be of great value.

[44] **Acknowledgments.** This paper has benefited enormously by thoughtful and constructive reviews by W. Kiefer and F. Nimmo, whose detailed comments led to a vastly improved manuscript. A.M.J. acknowledges support from the Canadian Institute for Advanced Research and NSERC during completion of this study. This work was supported under NASA Planetary Geology and Geophysics grants NNG05GK34G (to C.L.J.) and NNG066670G (to G.S.).

References

Agee, C. B., and D. S. Draper (2004), Experimental constraints on the origin of Martian meteorites and the composition of the Martian mantle, *Earth Planet. Sci. Lett.*, *224*, 415–429.

Arkani-Hamed, J. (2000), Strength of Martian lithosphere beneath large volcanoes, *J. Geophys. Res.*, *105*, 26,713–26,732.

Arkani-Hamed, J. (2004), Timing of the Martian core dynamo, *J. Geophys. Res.*, *109*, E03006, doi:10.1029/2003JE002195.

Bertka, C., and J. R. Holloway (2004), Anhydrous partial melting of an iron-rich mantle I: Subsolidus phase assemblages and partial melting phase relations at 10 to 30 kbar, *Contrib. Mineral. Petrol.*, *115*, 313–322.

Bibring, J.-P., et al. (2006), Global mineralogical and aqueous Mars history derived from OMEGA/Mars Express data, *Science*, *312*, 400–404.

Bills, B. G., G. A. Neumann, D. E. Smith, and M. T. Zuber (2005), Improved estimate of tidal dissipation within Mars from MOLA observations of the shadow of Phobos, *J. Geophys. Res.*, *110*, E07004, doi:10.1029/2004JE002376.

Bouvier, A., J. Blichert-Toft, J. D. Vervoort, and F. Albarede (2005), The age of SNC meteorites and the antiquity of the Martian surface, *Earth Planet. Sci. Lett.*, *240*, 221–233.

Christensen, P. (2005), The many faces of Mars, *Sci. Am.*, *293*, 32–39.

Comer, R. P., S. C. Solomon, and J. W. Head (1985), Mars: Thickness of the lithosphere from tectonic response to volcanic loads, *Revs. Geophys.*, *23*, 61–92.

Cordery, M. J., and I. H. Campbell (1997), Genesis of flood basalts from eclogite-bearing mantle plumes, *J. Geophys. Res.*, *102*, 20,179–20,197.

Crisp, J. A. (1984), Rates of magma emplacement and volcanic output, *J. Volcanol. Geotherm. Res.*, *20*, 177–211.

Daradich, A., J. X. Mitrovica, I. Matsuyama, J. T. Perron, M. Manga, and M. A. Richards (2008), Equilibrium rotational stability and figure of Mars, *Icarus*, *194*, 463–475.

Davies, G. F. (1994), Thermomechanical erosion of the lithosphere by mantle plumes, *J. Geophys. Res.*, *99*, 15709–15722.

Dunlop, D. J., and J. Arkani-Hamed (2005), Magnetic minerals in the Martian crust, *J. Geophys. Res.*, *110*, E12S04, doi:10.1029/2005JE002404.

Farnetani, C. G., and M. A. Richards (1995), Thermal entrainment and melting in mantle plumes, *Earth Planet. Sci. Lett.*, *136*, 251–267.

Forget, F., and R. T. Pierrehumbert (1997), Warming early Mars with carbon dioxide clouds that scatter infrared radiation, *Science*, *278*, 1273–1276.

Gonnermann, H. M., A. M. Jellinek, M. A. Richards, and M. Manga (2004), Modulation of mantle plumes and heat flow at the core-mantle boundary by plate-scale flow: Results from laboratory experiments, *Earth Planet. Sci. Lett.*, *226*, 53–67, doi:10.1016/j.epsl.2004.07.021.

Greeley, R., and B. D. Schneid (1991), Magma Generation on Mars: Amounts, rates, and comparisons with Earth, Moon, and Venus, *Science*, *15*, 996–998.

Griffiths, R. W. (1986), Thermals in extremely viscous fluids, including the effects of temperature-dependent viscosity, *J. Fluid. Mech.*, *166*, 115–138.

Griffiths, R. W., and I. H. Campbell (1991), Interaction of mantle plume heads with the Earth's surface, *J. Geophys. Res.*, *96*, 18,295–18,310.

Harder, H., and U. Christensen (1996), A one-plume model of Martian mantle convection, *Nature*, *380*, 507–509.
Harrison, K. P., and R. E. Grimm (2002), Controls on Martian hydrothermal systems: Application to valley network and magnetic anomaly formation, *J. Geophys. Res.*, *107*(E5), 5025, doi:10.1029/2001JE001616.
Hartmann, W. K., and G. Neukum (2001), Cratering chronology and the evolution of mars, *Space Sci. Rev.*, *96*, 165–194.
Hauck, S. A., and R. J. Phillips (2002), Thermal and crustal evolution of Mars, *J. Geophys. Res.*, *107*(E7), 5052, doi:10.1029/2001JE001801.
Heller, D.-A., and P. Janle (2000), Lineament analysis and geophysical modeling of the Alba Patera region on Mars, *Earth Moon Planets*, *84*, 1–22.
Jakosky, B. M., and R. J. Phillips (2001), Mars' volatile and climate history, *Nature*, *412*, 237–244.
Jellinek, A. M., and D. J. DePaolo (2003), A model for the origin of large silicic magma chambers: Precursors of caldera-forming eruptions, *Bull. Volcanol.*, *65*, 363–381.
Jellinek, A. M., and M. Manga (2002), The influence of a chemical boundary layer on the fixity, spacing and lifetime of mantle plumes, *Nature*, *418*, 760–763.
Jellinek, A. M., and M. Manga (2004), Links between long-lived hot spots, mantle plumes, D″, and plate tectonics, *Rev. Geophys.*, *42*, RG3002, doi:10.1029/2003RG000144.
Jellinek, A. M., H. M. Gonnermann, and M. A. Richards (2003), Plume capture by divergent plate motions: Implications for the distribution of hotspots, geochemistry of mid-ocean ridge basalts, and estimated of the heat flux at the core-mantle boundary, *Earth Planet. Sci. Lett.*, *205*, 361–378.
Johnson, C. L., and R. J. Phillips (2005), Evolution of the Tharsis region of Mars: Insights from magnetic field observations, *Earth Planet. Sci. Lett.*, *230*, 241–254.
Kerr, R. C., and C. Mriaux (2004), Structure and dynamics of sheared mantle plumes, *Geochem. Geophys. Geosyst.*, *5*, Q12009, doi:10.1029/2004GC000749.
Kiefer, W. S. (2003), Melting in the Martian mantle: Shergottite formation and implications for present-day mantle convection on Mars, *Meteorit. Planet. Sci.*, *38*, 1711–1875.
Kohlstedt, D. L., B. Evans, and S. J. Mackwell (1995), Strength of the lithosphere: Constraints imposed by laboratory experiments, *J. Geophys. Res.*, *100*, 17,587–17,602, doi:10.1029/95JB01460.
Langlais, B., M. E. Purucker, and M. Mandea (2004), Crustal magnetic field of Mars, *J. Geophys. Res.*, *109*, E02008, doi:10.1029/2003JE002048.
Lillis, R. J., et al. (2008a), Giant impacts and the death of the Martian dynamo: Where data meet models, *Lunar Planet. Sci.*, *XXXIX*, Abstract 1173.
Lillis, R. J., et al. (2008b), Magmatic history of southwestern Tharsis: Clues from volcanic history, thermo-magnetic modeling and electron reflection magnetometry, *Lunar Planet. Sci.*, *XXXIX*, Abstract 1159.
Lithgow-Bertelloni, C., M. A. Richards, R. W. Griffiths, and C. Conrad (2001), Plume generation in natural thermal convection at high Rayleigh and Prandtl numbers, *J. Fluid Mech.*, *434*, 1–21.
Loper, D. E., and F. D. Stacey (1983), The dynamical and thermal structure of deep mantle plumes, *Phys. Earth Planet. Inter.*, *33*, 304–317.
Manning, C. V., C. P. McKay, and K. J. Zahnle (2006), Thick and thin models of the evolution of carbon dioxide on Mars, *Icarus*, *180*, 38–59.
McGovern, P. J., S. C. Solomon, D. E. Smith, M. T. Zuber, M. Simons, M. A. Wieczorek, R. J. Phillips, G. A. Neumann, O. Aharonson, and J. W. Head (2002), Localized gravity/topography admittance and correlation spectra on Mars: Implications for regional and global evolution, *J. Geophys. Res.*, *107*(E12), 5136, doi:10.1029/2002JE001854. (Correction to "Localized gravity/topography admittance and correlation spectra on Mars: Implications for regional and global evolution," J. Geophys. Res., 109, E07007, doi:10.1029/2004JE002286, 2004.)
McKenzie, D., D.-N. Barnett, and D. N. Yuan (2002), The relationship between Martian gravity and topography, *Earth Planet. Sci. Lett.*, *195*, 1–16, doi:10.1016/S0012-821X(01)00555-6.
Musselwhite, D. S., H. A. Dalton, W. S. Kiefer, and A. H. Treiman (2006), Experimental petrology of the basaltic shergottite Yamato-980459: Implications for the thermal structure of the Martian mantle, *Meteorit. Planet. Sci.*, *41*, 1271–1290.
Neumann, G. A., M. T. Zuber, M. A. Wieczorek, P. J. McGovern, F. G. Lemoine, and D. E. Smith (2004), Crustal structure of Mars from gravity and topography, *J. Geophys. Res.*, *109*, E08002, doi:10.1029/2004JE002262.
Nimmo, F. (2000), Dike intrusion as a possible cause of linear Martian magnetic anomalies, *Geology*, *28*, 391–394.
Nimmo, F., and M. S. Gilmore (2001), Constraints on the depth of magnetized crust on Mars from impact craters, *J. Geophys. Res.*, *106*, 12,315–12,323.
Nimmo, F., and D. Stevenson (2000), The influence of plate tectonics on the thermal evolution and magnetic field of Mars, *J. Geophys. Res.*, *105*, 11,969–11,980.
Ogawa, Y., and M. Manga (2007), Thermal demagnetization of Martian upper crust by magma intrusion, *Geophys. Res. Lett.*, *34*, L16302, doi:10.1029/2007GL030565.
Olson, P., G. Schubert, C. Anderson, and P. Goldman (1988), Plume formation and lithosphere erosion: A comparison of laboratory and numerical experiments, *J. Geophys. Res.*, *93*, 15,065–15,084.
Olson, P., G. Schubert, and C. Anderson (1993), Structure of axisymmetric mantle plumes, *J. Geophys. Res.*, *98*, 6829–6844.
O'Neill, C., A. Lenardic, A. M. Jellinek, and W. S. Kiefer (2007), Melt propagation and volcanism in mantle convection simulations, with applications for Martian volcanic and atmospheric evolution, *J. Geophys. Res.*, *112*, E07003, doi:10.1029/2006JE002799.
Perron, J. T., J. X. Mitrovica, M. Manga, I. Matsuyama, and M. A. Richards (2007), Evidence for an ancient Martian ocean in the topography of deformed shorelines, *Nature*, *447*, 840–843.
Phillips, R. J., et al. (2001), Ancient geodynamics and global-scale hydrology on Mars, *Science*, *291*, 2587–2591, doi:10.1126/science.1058701.
Richards, M. A., and B. H. Hager (1984), Geoid anomalies in a dynamic Earth, *J. Geophys. Res.*, *89*, 5987–6002.
Roberts, J. H., and S. Zhong (2004), Plume-induced topography and geoid anomalies and their implications for the Tharsis rise on Mars, *J. Geophys. Res.*, *109*, E03009, doi:10.1029/2003JE002226.
Schubert, G., C. T. Russell, and W. B. Moore (2000), Timing of the Martian dynamo, *Nature*, *408*, 666–667.
Schubert, G., D. L. Turcotte, and P. Olson (2001), *Mantle Convection in the Earth and Planets*, 940 pp., Cambridge Univ. Press, New York.
Schultz, R. A., C. H. Okubo, C. L. Goudy, and S. J. Wilkins (2004), Igneous dikes on Mars revealed by Mars Orbiter Laser Altimeter topography, *Geology*, *32*, 889–892.
Smrekar, S. E., G. E. McGill, C. A. Raymond, and A. M. Dimitriou (2004), Geologic evolution of the Martian dichotomy in the Ismenius area of Mars and implications for plains magnetization, *J. Geophys. Res.*, *109*, E11002, doi:10.1029/2004JE002260.
Solomatov, V. S., and L.-N. Moresi (2000), Scaling of time-dependent stagnant lid convection: Application to small-scale convection on Earth and other terrestrial planets, *J. Geophys. Res.*, *105*, 21,795–21,817.
Solomon, S. C., et al. (2005), New perspectives on ancient Mars, *Science*, *307*, 1214–1220.
Stevenson, D. J. (2001), Mars' core and magnetism, *Nature*, *412*, 214–219.
Tanaka, K. L., D. H. Scott, and R. Greeley (1992), Global stratigraphy, in *Mars*, edited by H. H. Kiefer et al., 345–382, Univ. of Ariz. Press, Tucson.
Turcotte, D. L., R. J. Willemann, W. F. Haxby, and J. Norberry (1981), Role of membrane stresses in the support of planetary topography, *J. Geophys. Res.*, *86*, 3951–3959.
Wanke, H., and G. Dreibus (1994), Chemistry and accretion history of Mars, *Philos. Trans.R. Soc. London, Ser. A*, *349*, 285–293.
Watts, A. B. (2001), *Isostasy and Flexure of the Lithosphere*, 458 pp., Cambridge Univ. Press, Cambridge, U.K.
Wenzel, M. J., M. Manga, and A. M. Jellinek (2004), Tharsis as a consequence of Mars' dichotomy and layered mantle, *Geophys. Res. Lett.*, *31*, L04702, doi:10.1029/2003GL019306.
Williams, J.-P., and F. Nimmo (2004), Thermal evolution of the Martian core: Implications for an early dynamo, *Geology*, *32*, 97–100.
Williams, J.-P., F. Nimmo, W. B. Moore, and D. A. Paige (2008), Formation of Tharsis on Mars: What the line-of-sight gravity is telling us, *J. Geophys. Res.*, doi:10.1029/2007JE003050, in press.
Zhong, S., and J. H. Roberts (2003), On the support of the Tharsis rise on Mars, *Earth Planet. Sci. Lett.*, *214*, 1–9.
Zhong, S., and M. T. Zuber (2001), Degree 1 mantle convection and the crustal dichotomy on Mars, *Earth Planet. Sci. Lett.*, *189*, 75–84.
Zuber, M. T., et al. (2000), Internal structure and early thermal evolution of Mars from Mars Global Surveyor topography and gravity, *Science*, *287*, 1788–1793.

A. M. Jellinek and C. L. Johnson, Department of Earth and Ocean Sciences, University of British Columbia, 6339 Stores Road, Vancouver, BC M5S 1A7, Canada. (mjellinek@eos.ubc.ca)

G. Schubert, Department of Earth and Space Sciences, University of California, 595 Charles Young Drive East, Box 951567, Los Angeles, CA 90095-1567, USA.